IMAGING TUMOR USING POSITRON EMITTERS

Alshebani Alzarough

A thesis submitted in partial fulfillment of
the requirements for the degree of
Master of Science

Department of Physics

Central Michigan University
Mount Pleasant, Michigan
December, 2012

Accepted by the Faculty of the College of Graduate Studies,

Central Michigan University, in partial fulfillment of

the requirements for the master's degree

Thesis Committee:

Committee Chair

Faculty Member

Faculty Member

Date: 8-15-2012

Dean
College of Graduate Studies

Date: 11/15/12

Committee:

Mihi Horoi, Ph.D., Chair

Valeri Petkov, Ph.D.

Joseph Finck, Ph.D.

ACKNOWLEDGMENTS

I would like to express my gratefulness and special thanks to my advisor, Dr. Mihai Horoi, for his support and guidance through this project and throughout my research career at Central Michigan University. I would also like to stretch my thanks to Dr. Valeri Petkov and Dr. Joseph Finck for reading the drafts of this document and giving the suggestions to put this work in its final stage. Also, I would like to give my sincere gratitude and thanks to my family and my friend who gave me the comfort and support throughout my career. Finally, I would like to give my thanks to the Physics Department and Central Michigan University for giving me the opportunity and support to do this work.

ABSTRACT

IMAGING TUMORS USING POSITRON EMITTERS

by Alshebani Alzarough

In nuclear medicine imaging, Positron Emission Tomography (PET) is a technique that produces three-dimensional images of functional processes in the body. These images are derived from the metabolic activities of the radiopharmaceuticals absorbed by the tissue under study. The PET system detects (in coincidence) the pairs of gamma-rays (γ-rays) that are emitted in opposite directions in order to reconstruct the source using the standard techniques. The increase in access to PET and computed tomography (CT), has resulted in a major change towards using functional imaging as tool for tumor detection. Determining the size and location of cancerous tumors is usually achieved using PET with high accuracy. The computer simulations that have been carried out in this project are done using a Monte Carlo Method for particle transport implemented in FLUKA Code. A positron source (cancerous tumor) was simulated inside the body in order to reconstruct the volume and the position of this source, which depends on the accumulation of the radioisotope. I used the lines of response (LOR) as measure of γ-ray fluence flowing out of the region where the positrons have high concentration in order to trace back the position of the annihilation events. In radio-diagnosis, reasonable image resolution may require a higher dose, and this may result in secondary cancer. The biological dose in the regions surrounding the positron source is calculated and the results are compared to the experimental data.

TABLE OF CONTENTS

LIST OF TABLES

TABLE PAGE

LIST OF FIGURES

CHAPTER I

INTRODUCTION

1.1 An Introduction to Emission Tomography

Emission tomography (ET) is a branch of nuclear medical imaging that enclose two main techniques: positron emission tomography (PET) and single-photon emission computed tomography (SPECT). In both techniques, radioactive materials are used in order to enable the physician to visualize the properties of the body's physiology. For instance, spatial distribution of properties such as blood flow, glucose metabolism can be represented using ET techniques. Therefore, doctors can use ET techniques to detect cancerous tumors, and identify regions of the brain that are influenced by drugs. ET techniques fall under functional imaging category as compared to some other medical imaging techniques such as x-ray computed tomography (CT) that depicts the anatomy of the body [1, p. 11]. In functional imaging, the changes in metabolism, blood flow, and regional chemical compositions are detected or measured [2, ch.2]. PET can be combined to give a full descriptive image of the body. Figure 1.1 shows how the anatomical depiction of the body using CT can be combined with the PET's functional processes representation to give clear image of the body. [1, p. 13]. The term emission tomography defines the correlation between two principles: using γ-ray emission for imaging, in which the photons are traced and volumetric imaging of the body's interior. In ET, the radiotracer distribution inside the body is visualized with two main principles: projection imaging and tomography. The principle of projection imaging represents an image as it is seen by an observer looking through the body from outside. Where in tomography, the tomographic image represents cross-sectional slices of the body, and a pile of these cross-sectional slices will give the volumetric image. In ET, generally,

scanning data are recorded in the form of projections and then analyzed for image reconstruction using some standard techniques discussed in section 1.3.4.

Visualization of PET/CT protocol

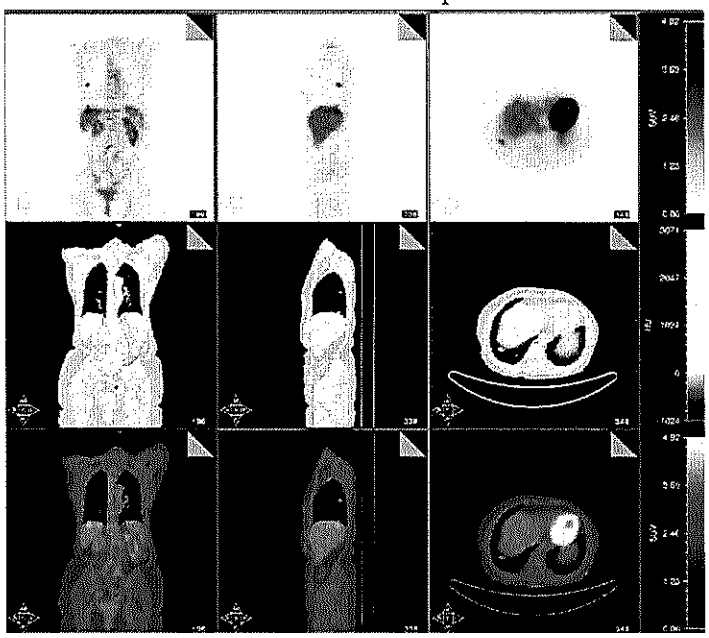

Figure 1.1. Figure taken from [1, p. 204].

1.2 Positron Emission Tomography (PET)

Positron emission tomography (PET) is a nuclear medicine imaging technique that depends on the detection of photons (two γ-rays) resulting from the annihilation of positrons emitted by a radionuclide (tracer). These two γ-rays are detected in coincidence. Since these two γ-rays go in opposite directions (180^o), the position where the annihilation has occurred can be determined with high precision. One of the main reasons for PET importance in medical research and clinical application is that positron-emitting isotopes of elements, such as fluorine, nitrogen, and oxygen, and, can be processed to create a range of radiopharmaceutical compounds (tracers) that are similar to those substances naturally occurring in the body. Originally, PET was primarily used as a research tool and has become one of the most important nuclear medicine imaging techniques in the recent years. It has a wide

range of clinical uses in oncology, such as detecting cancerous tumors at early stages and studying their resurrection after preforming treatment. The most commonly used radiotracer in oncology is 18F-fluoro-deoxy-glucose ($^{18-}$F-FDG). It is widely used in such application because it is easy to synthesize with a high radiochemical yield [3]. What makes $^{18-}$F-FDG ideal for imaging in oncology, is that cancer cells absorb more glocouce and use it as an energy source than normal cells [4, p. 371]. Also, it has an appropriate half-life time of 110 minutes as compared to some other radionuclides used in PET system, see table 1.1. This will give enough time for $^{18-}$F-FDG to be distributed in the body.

1.3 Physical Principles of PET Scan

What makes PET a unique and an appropiate medical imaging method among some other methods such as, CT and magnetic resonance imaging (MRI), is that PET has some advantages of using some of the physical principles that are basically the main concepts of its imaging techniques, such as, positron annihilation, γ-rays (photons) detection in coincidence, and the interaction of these photons with human tissue. These priciples are discussed in the following sections.

1.3.1 Positron Emission and Annihilation

Some isotopes that are proton-rich may decay via positron emission, in which a proton in the nucleus is converted into a neutron, resulting in the emission of positron and neutrino. Table1.1 lists some examples of isotopes that decay via positron emission [5, p. 18]. In PET, some of these radionuclide are labeled to some certain compounds such as glucose to creat what called a radiopharmaceutical tracer. An example of these radiopharmaceutical tracers is Fluorine- Dioxide Glucose (^{18}F-DG), in which the fluorine will undergo beta decay, decaying to Oxygen:

$$^{18}\mathrm{F} \rightarrow ^{18}\mathrm{O} + e^{+} + \nu + Q \tag{1.1}$$

where Q is the decay released energy and it is different in value from one isotope to another. As it can be seen from the table 1.1 that the $^{18-}$F is one of the most common and appropriate radionuclide label used in PET imaging since the emitted positron has a law maximum energy and a small mean range as compared to the other radionuclides.

Table 1.1. Some common radionuclides used in PET. $T_{1/2}$ is the half-life time for the radionuclide, β^+ is the decay mode (emitting positrons), E_{max} (MeV) is the average maximal energy of beta decay, e^+range (mm) is the average range that the positrons resulting from (β^+ decay) travel before they lose their energy and come to rest. Table taken from [5, p. 19].

Radionuclide	Daughter	$T_{1/2}$(mins)	β^+ (%)	E_{max} (MeV)	e^+range (mm)
Rubidium-81	$^{81-}$Kr	1.3	96	3.35	2.6
Gallium-68	$^{69-}$Zn	68.0	88	1.89	1.9
Oxygen-15	$^{15-}$N	2.1	100	1.72	1.5
Nitrogen-13	$^{13-}$C	10.0	100	1.19	1.4
Carbon-11	$^{11-}$B	20.4	99	0.96	0.3
Fluorine-18	$^{18-}$O	110.0	97	0.64	0.2

Positrons lose their kinetic energy as they travel through human tissue through different interactions, such as Coulomb interactions with electrons, and Compton scattering. Since the positron and electron have the same rest mass, their direction may get deviated as they lose their kinetic energy, during positron's Coulomb interactions with electrons. Positrons start to interact with electrons at thermal energies via annihilation in which two 511 (keV) photons are produced in opposite direction or by forming hydrogen-like orbiting couple called positronium. In the ground state, positronium has two forms: ortho-positronium and para-positronium. In ortho-positronium, the electron and positron have parallel spins, where in para-positronium, the spins are anti-parallel. Para-positronium decays via self-annihilation, resulting in the emission of two 511 keV photons in opposite directions. In ortho-positonium, the self-annihilation decay produces three photons. Both positronium forms are receptive to the pick-off process, where the positron annihilates with another electron. Over 80% of the decay

events are because of free annihilation and the pick-off process. There is an angular uncertainty in the direction of the two 511 keV photons if the momentum of the interacting particles (electron and positron) in the free annihilation and pick-off processes is varied. This uncertainty is about 4 mrad in the observer's frame. Also, there is a characteristic positional inaccuracy that arises from the finite range of the positrons as well as the non-collinearity of the two 511 keK photons resulted from the annihilation. It is about 2-3 mm for a PET camera of diameter 1 m and transaxial field of view of 0.6 m [3].

1.3.2 Coincidence Detection

In principle, when a PET scanner registers an incident photon, each detector generates a timed pulse. In order to register the coincidence events, these pulses are linked in a circuit that has short time-window (7-15) nanoseconds. When a photon hits a detector, this will open a time window for about 15 ns, and if another photon hit another detector that is linked to the same circuit within this time-window, the system will be considered it as a coincidence event [5, 6]. A conceptualized diagram of this process is shown in Figure 1.2.

The line that is connecting two detectors in the coincidence circuit is called line of response (LOR). This helps with determining the positional information without the need for physical collimators. And this is what is called electronic collimation. As compared to the physical collimation, the electronic collimation helps to improve the sensitivity and the uniformity of the point source response function (psrf). The physics collimation are meant to prevent the photons that are not perpendicular or almost perpendicular to the collimator's face from falling on the detector, hence obtaining the directional information. On the other hand, these prevented photons could be detected and used as signal or pulse in electronic collimation. This will increase the sensitivity. And this what gives the PET method

and advantage over SPECT in regard of image resolution, 5-10 mm in PET and 15-20 mm in SPECT [3]. When it comes to a good coincidence counting efficiency, chosing the right material for the detec-

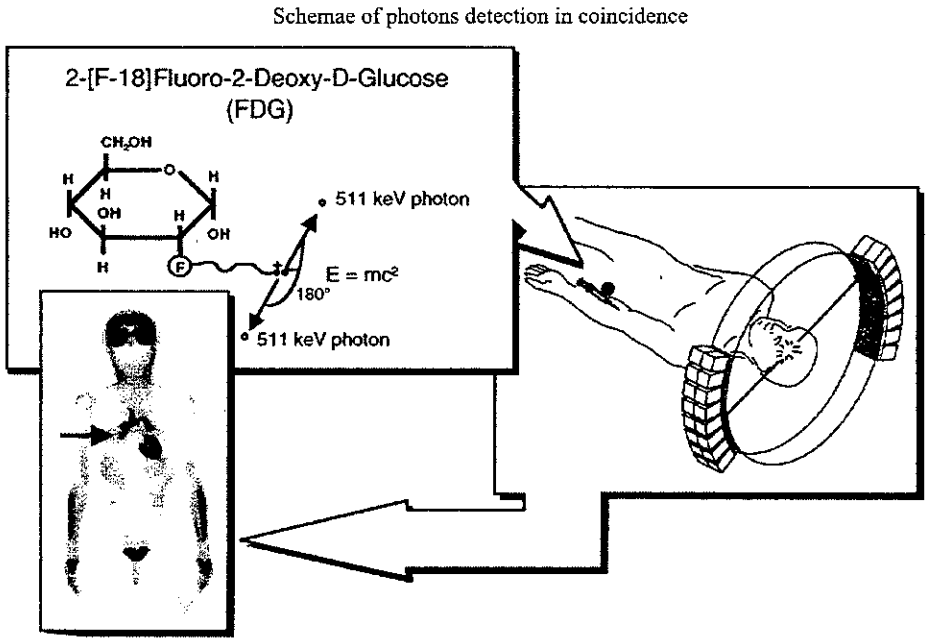

Figure 1.2. Pairs of γ-ray photons are detected in coincidence. Detectors are linked through coincidence circuit to ensure that the pairs are from the same annihilation event. Figure taken from [5, p. 2].

tors is very important. In PET system, solid scintillation detectors are used. Generally the choice of the detector material is based on: stopping power for 511 keV photons, scintillation decay-time, light output per keV of photon energy, and energy resolution of the detector. The stopping power is determined by the mean distance that a photon travels until it stops (its total energy is deposited). It depends on the density of the material as well as the effective atomic number. Scintillation decay time is the time required for an excited atom (of the detector material) to decay to the ground state, and and it has a relation with the dead time (time at which the detector is unable to register any hit). Decay time plays main role when considering the counting efficiency and it is normally given in nanoseconds (ns) [7].

For instance, bismuth gemanate (BGO) has decay time about 300 ns, and it's 40 ns for lutetium oxy-orthosilicate (LSO). Though the decay time for BGO is quite long (low couting rate) as compared to LSO, the over all for detector efficiency is evaluated by all other characteristics mentioned previously. The energy resolution is related the light-output. Better energy resolution means high-light-output. This character of scintillation (energy resolution) depends on the crystal structure of the detector [8, p. 5], [9, p. 20].

1.3.3 Types of coincidence events

There are four types of coincidence events in PET: true, scattered, random, and multiple. Figure 1.3 illustrates the these four types. In scattered coincidence, one or both of the detected photons undergo Compton scattering. Because the direction of the scattered photos is slightly or significantly changed during Compton scattering, these coincidence events may be assigned to the wrong line of response (LOR). This wrong assigning of LOR will add a background to those correlated to the true coincidence events, hence, decreasing the contrast and over estimating the concentration of the radionuclide. The statistical noise is usually increased by the number of the scattered events and this number is depends of the attenuation properties and the volume of the scanned object.

In random coincidence, the detected pairs of γ-rays are not from the same annihilation event even though they are detected within the time-window in the coincidence circuit. For a given LOR, the number of random coincidences is related to the rate of the events detected by the detectors linked by that LOR. The rate of the random coincidences is proportional to the square of the activity in the FOV. The number of the random coincidences depends on the characteristics of the imaged object such as volume and the attenuation. Also it depends on the geometry of γ-ray camera. This random number of coincidences is uniformly distributed across the FOV and will lead to an overestimation of isotope

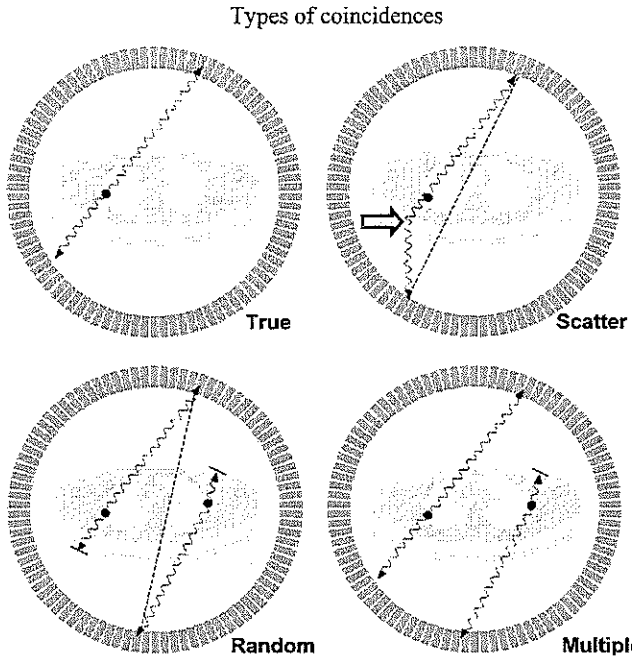

Figure 1.3. Schema of different types of coincidence events registered by PET system using a ring of detectors array. The position of positron annihilation is indicated by the black circle. Figure taken from [10, p. 42]

concentrations if it is not corrected. Random coincidences also contribute to the data as a statistical noise [3], [11, p. 210].

1.3.4 Image Reconstruction

The next step after the γ-ray data has been acquired is image reconstruction. There are several methods used for image reconstruction such as simple back projection and filtered back projection.

In the **simple backprojection** 2-D acquisition, for a given line of response (LOR) in a sinogram, the activity is given by the sum over all activities detected by a detector pair along the line through of the object. These LORs, are then used in the backprojection principle in order to reconstruct the images. The reconstructed images using backprojection are simply a matrix in a definite size (e.g., 200 ×200 pixels) in terms of cartesian coordinates (x,y). Whereas, the data in the sinogram is expressed in polar coordinates. The position of an image pixel in (x,y) is related to polar coordinates

shown in figure 1.4 by:

$$r = x\,sin\phi + y\,cos\phi \tag{1.2}$$

Equation (1.2), is used to calculate each image pixel (x,y) at projection angle ϕ. The corresponding measured counts in the projection sinogram for the calculated r, are added to the pixel (x,y) in the image reconstruction matrix. This is done for all projection angles and the backprojection image pixel A(x,y) in the reconstruction matrix is calculated by:

$$A(x,y) = \frac{1}{N}\sum_{N=1}^{N} p(r,\phi) \tag{1.3}$$

Where p(r, ϕ) is the count density (measured counts) in the sinogram element in the acquired matrix, and N is the number of projection angles.The reconstructed image will be the result of all computed pixels using simple backprojection method. [9, ch. 4].

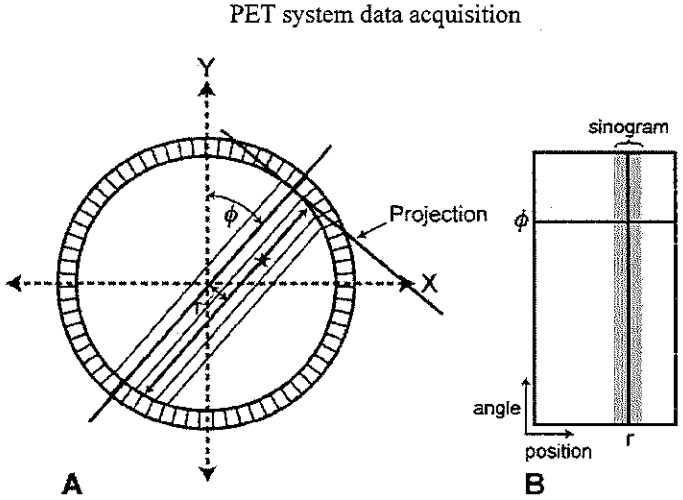

Figure 1.4. Aquisition of data in PET system. Data for all r and ϕ values that have been acquired in (A) are plotted in polar coordinates (r, ϕ) to produce sinogram indicated by the shaded area (B). Figure taken from[9, p. 14].

The **filtered backprojection** method (FBP), is one of the most common traditional approaches to image reconstruction from PET and SPECT data. It is a mathematical technique that uses an idealized model of PET and SPECT ignoring many significant properties of the real data. For instance, the number of detected γ-ray events traversing along a particular direction is approximated as an integral of radiotracer distribution along that line. Despite the fact that FBP does not consider some important effects, such as noise, attenuation, scatter, and blur, a reasonable images using this method can be obtained [1, p. 18].

The following chapter will disucss: some of the basic concepts in medical tomography to give an overview of some of the interactions of radiation with matter and theri relavent consequences such as, biological effects II. Chapter[III] will give a brief description about the Monte Carlo method in physics that is being implemented in FLUKA code, and the methology of the simulation will be addressed. Later, chapter [IV] will carry out the results' discussion and the coclusion.

CHAPTER II

BASIC CONCEPTS IN MEDICAL TOMOGRAPHY

2.1 Interaction of Radiations With Matter

Generally, radiations of charged particles such as α-particles, protons, β-particles, and non-charged particles (electromagnetic radiation), such as γ-rays, cause an excitation or ionization while they are passing through materials. These kinds of radiations are called ionizing radiations. These radiations are categorized into penetrating and non-penetrating radiations. Since penetrating radiations (photons) have no mass, they travel longer distance in material as compared to non-penetrating radiations with the same energy. Therefore, the interaction of these two types of radiation is relatively different and they have an important aspect in nuclear medicine imaging. In this project, γ-ray, electron (e^-), and positron (e^+) interactions with human tissue are discussed in the following sections since they are important in PET scan.

2.1.1 Gamma-ray Photons (γ)

There are three major types of γ-ray interactions with matter, photoelectric absorption, Compton scattering, and pair production. In PET imaging photoelectric effect and Compton scattering are of importance as biological effects. In general, γ-ray photons lose their energy via interaction with the electrons at the outer shells or the nucleus of the absorber atom. Photons of γ-ray may lose their total energy or some of it in a single encounter.

During the **photoelectric effect**, the interaction between a photon and an orbital electron of the absorber atom involves a complete absorption of the photon energy, resulting in ejection of that electron. The energy of this electron is given by:

$$E_e = E_\gamma - E_B \tag{2.1}$$

where E_γ is the energy of incident photon (emitted after the annihilation of tthe positron), and E_B is the biding energy for the electron.

Primarily, the photoelectric effect occurs when a penetrating photon through an absorber has low-energy range. Therefore, the probability of this effect decreases as the penetrating photon's energy increases. Also, this probability increases as the atomic number (Z) of the absorber increases. The photoelectric effect, is roughly proportional to $\frac{Z^5}{E_\gamma^3}$ [12, p. 332], [13, p. 61]. As can be seen from figure 2.1, the photoelectric effect occurs with higher percentages with K-shell electrons.

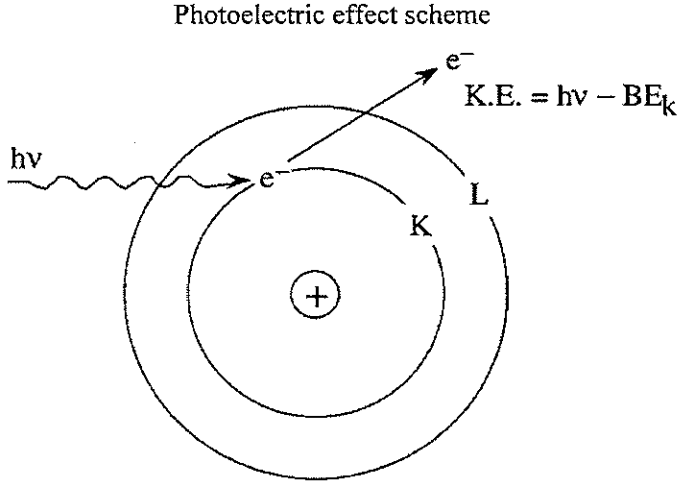

Figure 2.1. The photoelectric effect. It occurs primarily with K-shell electrons. Figure taken from [12, p. 332].

Typically, a characteristic x-ray will be emitted as a result of the transition of an electron at a higher energy level to fill the gap created in the K-shell. The ejected electron will, eventually, lose its energy via absorption during another photoelectric interaction. It is more likely that the emitted x-ray might be absorbed via another photoelectric interaction.

In **Compton scattering**, a part of a γ-ray energy is transferred to an electron in the outer shells of the absorber atom. This process involves an increase of the electron's energy and change in the photon's direction. as illustrated in figure 2.2.

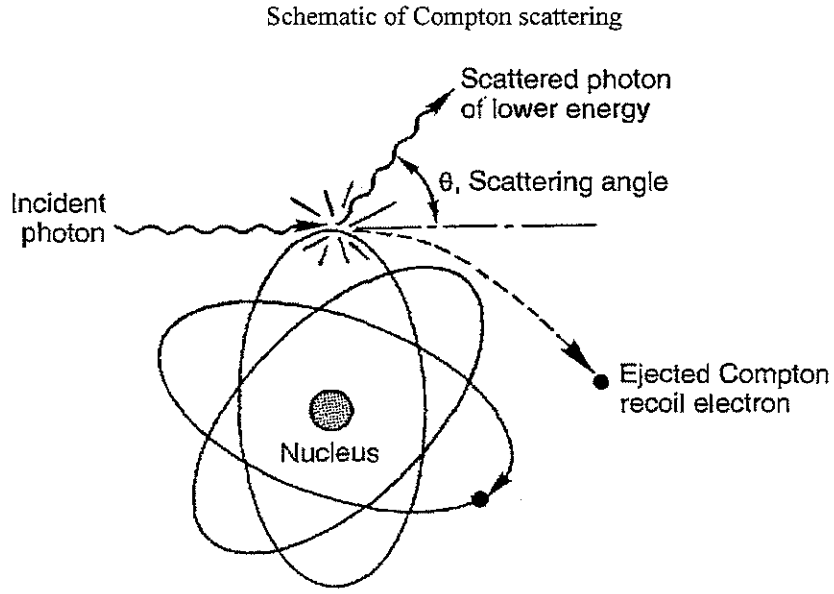

Figure 2.2. The Compton scattering. A part of the incident photon's energy is transfered to a Compton recoil electron. Figure taken from [14, p. 78].

From the law of conservation of energy and momentum, the energy of the scattered photon is given by:

$$E' = \frac{E}{1 + (E/m_0c^2)(1 - cos\theta)} \tag{2.2}$$

Where E is the energy of the incident photon, E' is the energy of the scattered photon, m_0 is the rest mass of the electron, c is the speed of light, and and θ is the scattering angle. From equation (2.2), one can see that there is a quite large deflection despite the small energy loss. Since a part of the

photon's energy is transferred to the electron, the energy of the recoil electron (E_{rec}) can be calculated from:

$$E_{rec} = E - E' \tag{2.3}$$

This energy (E_{rec}) does not depend on the properties of the absorbers material such as, density, atomic number, etc., [14, p. 78].

2.2 Charged Particles

Energetic charged particles such as, α particles and β particles, lose their energy while they pass through absorber material via interacting with the orbital electrons of the atoms in the material. During this process, an electron may get ejected leaving the atom ionized, or an electron is moved to a higher energy level leaving, the atom in an excited state. During these two processes (ionization and excitation), the chemical bond in molecules in the material may break, and that may lead to changing in the chemical entities. The path of the light charged particles like β particles (e^-, e^+) when they pass traverse through a material is a zigzag, whereas in heavy charged particles like α prticles, they have a straight path because of their heavy mass and charge [9, p. 10].

The straight-line path that a charged particle traverses in a medium is called the range R, and it depends on the energy of the charged particle, its mass, and the density of the medium. This range increases as the energy of the charged particle increases. It is inversely proportional to the increase in the mass of the charged particle as well as the density of the medium [13].

2.2.1 Electrons And Positrons

As charged particles, electrons and positrons are governed by electromagnetic forces such as the Coulomb force. In interactions that involve repulsive or attractive forces for particles of equal

mass, the impulse and transfer energies are about the same. This implies that the tracks in an absorber for positively charged electrons (e^+) or the normal electron (e^-) are similar. However, positrons are significantly different from electrons when it comes to annihilation radiation energy generated at the end of their track. What makes positrons ideal for medical functional imaging is that their mean range within the absorber is small as compared to other charged particles [15].

2.3 Dose Rate

In medical physics, dose rate is one of the most important concepts whether it is in radiation therapy or diagnosic purposes. The absorbed dose refers to the absorbed energy per unit mass of tissue [13, p. 209]. This energy is measured in joules and mass in kilograms. The IS unit of dose **D** is the gray (*Gy*). Thus:

$$1 \text{ Gy} = 1 \text{ Joule/Kg} \tag{2.4}$$

2.3.1 Dose Equivalent

The dose equivalent **H**, refers to the dose which gives the same risk of damage or detriment to health whatever the type of radiation, and it has the unit of Sievert (*Sv*). The dose equivalent is given by:

$$\mathbf{H} = \mathbf{D} \times \textit{constant}\,, \tag{2.5}$$

The *constant* is defined as the radiation-weighting factor, depending on the type of radiation. For instance, $\gamma-$ray photons have a constant of 1, and for neutrons and $\alpha-$particles it is 10 and 20 respectively. In its content, the dose equivalent has an important aspect since it varies with the radiation. Hence, the biological damage is different though the deposited energy might be the same. Therefore, the biological effects of radiation are not directly proportional to the amount of energy deposited by

radiation in a tissue. Biological effects due to radiation depend on the energy deposited by radiation as well as how this energy is distributed. The biological damage due to radiation is relatively increasing with the linear energy transfer(LET). Therefore, for low-LET radiation such as, γ-rays, β-particles, etc., the biological damage is less than that caused by high-LET radiation (eg., α particles, neutrons, etc.) for the same absorbed dose [12, ch. 14].

2.4 Biological Effect Due to Linear Energy Transfer

Linear energy transfer refers to the density of the energy deposited along the path of which a charged particle traversing an absorbing material. The LET is expressed as, KeV/μm, the energy deposited by radiation per unit length of the path traversed through the absorber material [16, p. 366]. When considering the effects from radiation caused to living tissue, the energy distribution is very important since the linear energy depends on it. That means low-LET radiation such as x-rays and γ-rays have less damage to the tissue as compared to the non-penetrating particles (e.g., α-particles, electrons, deuterons, etc.) as discussed in section 2.3.1.

The relative biological effectiveness is introduced (RBE) in order to compare the effect of different radiations. It is a dimensionless quantity, and it is defined as the ratio of the dose for given end point for a reference radiation to yield a certain biological response to yield the same biological response to the dose for given end point for the test radiation. Generally, x-ray radiations of 250 KeV are chosen as reference radiation (standard radiation) because of their common use. Figure 2.3 illustrates the relation between the RBE and LET [13, p. 209]. The *optimal* LET, refers to the value of LET that produces biological effects. From figure 2.3, one can see that 100 KeV/μm is an optimal LET. This is because the average separation between ionizing events at this density of ionization, almost coincides with the diameter of the DNA double helix (2 nm). Therefore, any ionizing radiation

with this density of ionization tends to have a high probability of causing double-strand break in which both strands in the double helix are severely damaged [17, p.112].

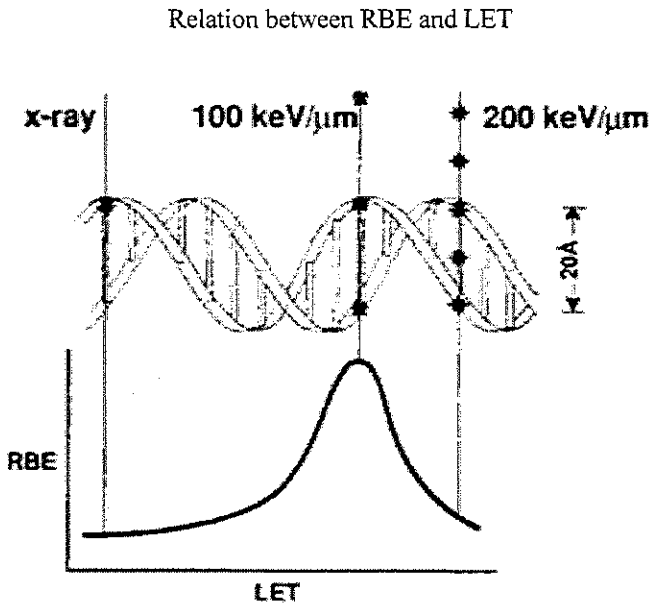

Figure 2.3. RBE versus LET. The diagram shows that a LET of 100KeV/μm has the greatest RBE for cell killing, mutagenesis, or oncogenic transformation. Figure taken from [17, p .112].

CHAPTER III

MONTE CARLO METHOD FOR PARTICLE TRANSPORT SIMULATION

3.1 Monte Carlo Method and Particle Transport

In physics, there are many processes that are stochastic (having a random distribution or pattern). That means, one cannot infer a prediction from previous observation of an event how the next one would be even though the starting conditions are the same. Particle transport is one of these processes. These processes are usually described using Monte Carlo method. There are two main components in Monte Carlo method, random numbers and probability. A random is a number in a sequence of numbers, which cannot be predicted from the previous or the next number in the sequence. A probability refers to how likely an event may occur. In particle transport physics, the probability is related to the occurring of an interaction of particles (charged and uncharged) as they traverse through matter. The probability of these interactions is described by the cross section [18].

For a computer simulation, I used the FLUKA Code. It is a particle physics Monte Carlo simulation package for particle transport and interactions with matter. It has a wide range of applications starting from proton-electron accelerator shielding to detectors design, such as neutron detectors. Also it is used for calorimetery, dosimetry, cosmic rays, neutrino physics, and radiography applications. In the medical field and radiation safety, it has been used for dose calculation of external radiations. For more realistic and reliable estimation regarding dose calculation and radiation safety, it contains a library of the International Commission on Radiological Protection (ICRP) information. With high accuracy, FLUKA can simulate the interaction of different material with matter for about 60 different particles, photons and electrons included, with energy ranges from 1 keV to thousands of TeV [19].

Like any computer simulation package, the input file of FLUKA has some important structures that have to be addressed, such as geometry, material, detectors, physics, particles transport (sources), etc. These structures are introduced through command cards. The FLUKA code is faciliated through graphical user interface (GUI) called "flair", that enables users to easily edit the FLUKA input file, and also, users can now visuilaze the geometry and the output files. For 3D visualization of the simulation set up (input file geometry) SimpleGeo is a user graphical tool that can be used to visualaize the geometry as well as some of the results, such as the Bragg peak and energy distribution.

3.2 Method

The set up of the simulation mainly focuses on simulating a positron source located at different positions inside a body phantom. For the body phantom, we used water since the human body is about 70% water. In a practical PET scan system the γ-ray's camera is made of sets of coaxial ring array detectors. Each detector elemnt is linked (in a coincidence circuit that has time-window of 6-20 ns) with a cetain number of detectors. This number is normally chosen to be N/2; where N is the total number of detectors in each ring array detector [9, p. 27]. Figure 3.1 illustrates a ring detectos shows how each detector is linked in a fashion of N/2. In this project, the γ-ray's camera is a square detector array having 20 detectors on each side as illustrated in figure 3.2. The length of each side of the square detector array is configurd to be 100 cm. In this project, each detector element in a specific side of the square array is linked (in a coinceidence circuit) with all other detectors in the neighboring sides. This is done to account for all possible coincidences events. For the detector material, first I used Silicon (for the first three differernt location) and then Bismoth Germinate Oxidise (BGO). It was found that the use of BGO as material gives a more reasonable signal as compared to the silicon. This high signal can be related to the fact that the BGO has a very short dead time. As discussed earlier in the section

Arrangement of Detectors

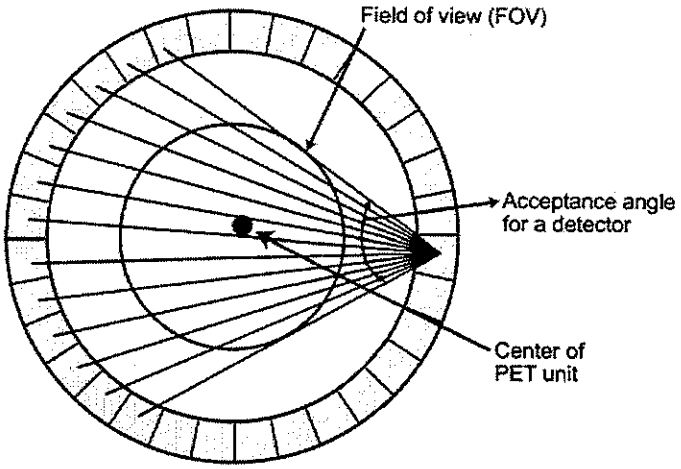

Figure 3.1. Each detector is connected in coincidence with a half total number of detectors in the ring. Figure take from [9, p. 27].

1.3.2, dead time for the scinitilation detectors is an important aspect when it comes to counting the number of coinicidence events. Each detector element in the square detector array has a thickness of 4 cm, width of 5 cm, and height of 20 cm. The hight of the detectors is quite big. This was chosen to detect as much number of coincidence as possible. The body phanton has dimensions of (40 cm $\times$30 cm $\times$ 20 cm), and it is located at the center.

Fluoride dioxide glucose (^{18}FDG), is one of the most common and appropriate radinuclide used in PET. It has a wide range of use in PET imaging such as, epilepsy, dementia, primary tumors metastates diagnoses, etc. For our simulation, the energy of the a positron source was set up to be 0.634 MeV since ^{18}FDG has a maximum and an average positron energy of 0.634 MeV and 0.202 MeV respectively [4, 11].

In the second step of this project, I calculated the dose equivalent and compared to the ICRP regulations for conversion coefficients for radiological protection quantities for external radiation exposures. For better image resoultion, a high dose might be rquired and this may rise the increase of getting secondary cancers. According to ref. [20], for combined PET/CT scanners CT conponent contributes with about 81% of the total dose. In this project, the dose equivalent is calculated bassed on full-scan time of 20 minutes. The dose equivalent calculation is described in Appendix B and the results are discussed in section 4.2.

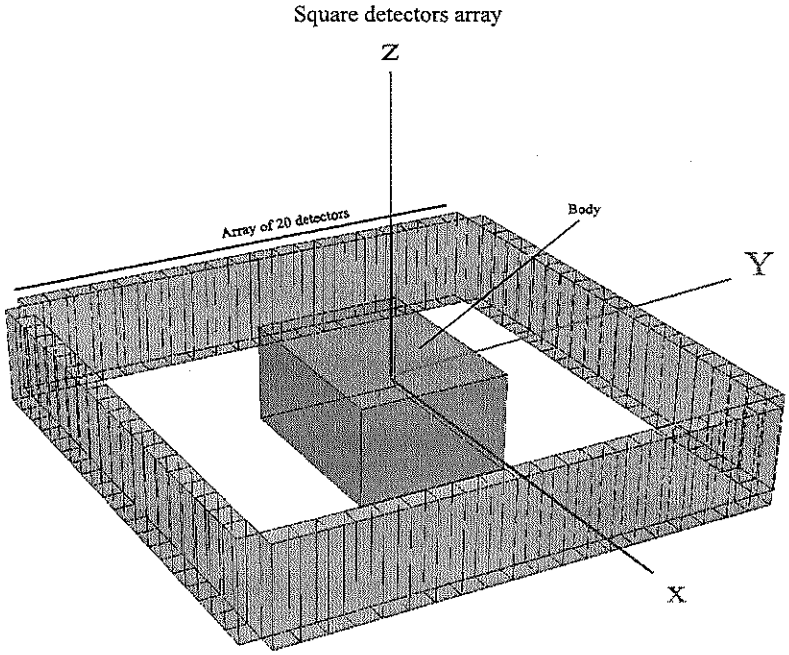

Figure 3.2. The square detector array and the body phantom both are located at the center of the geometry reference frame.

CHAPTER IV

RESULTS AND DISCUSSION

4.1 Source Reconstruction

After the data of the simulation has been collected, the position and the size of the positron source is reconstructed by calculating the line segments that cross each cell on the grid shown in figure 4.1. These line segments are represented as a measure of γ-ray fluence contributions. The fluence defined by the number of particles per unit area ($1/m^2$). To envision how the lines of response on the

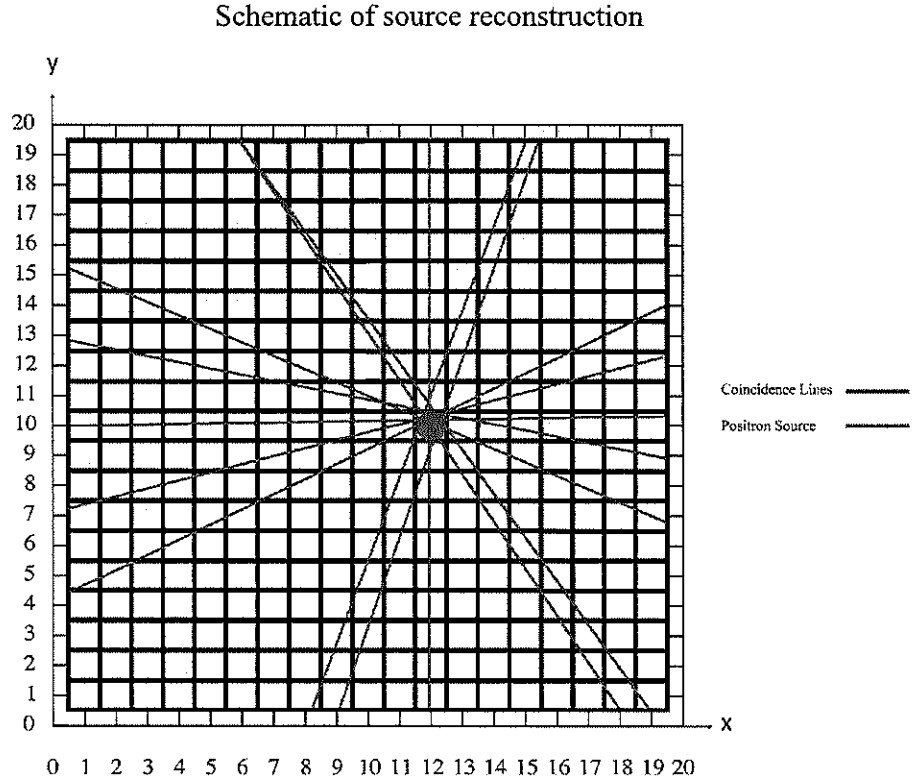

Figure 4.1. Schematic of source position and size reconstruction. Each red line represents the line of response (coincidence event).

grid contribute the cells on the grid, figure 4.1 shows that each line that is passing through the positron source is crossing a part of the squares (cells on the grid) along its path. This (line segment) is counted

as a contribution to the crossed cell with respect to its length. That means, the longer line segment (of a particular cell), has more contribtion to that cell on the grid. The line segments of each line on the grid were calculated using a fortran code. Another fortran code is used to extract the coordinates of the lines of resposnse and use them them as an input to the line segments calculation code. The position where the coincidence event has occured is related to the line of response (LOR) that connects the two detectors. As one can see from figure 4.2, this line passes through the region where a high concentration of positrons is exhibited. This is true since the positron travels a short distance (few millimeters), see table 1.1, before it is annihilated. The position where the positron source is located, is related to the peak of γ-ray fluence contributions in the plots. In other words, the spot where the peak is located exibits a high concentration of positrons.

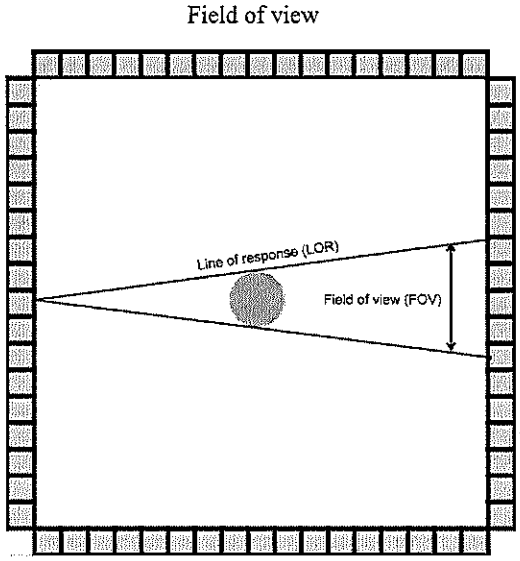

Figure 4.2. Field of view (FOV) for the square array detector. Line of response is the line that connects two detectors in the coincidence circuit.

To illustrate the distribution of the positron source where it has a high concentration, the sum over γ-ray fluence contributions to each cell are ploted using a contour plot. The first three simulations

were done using silicon for the detector material. First, I positioned the positron source at the center of the body phantom (10,10,0.0).The body phantom is positioned at the center of the square detector array, see figure 3.2. As can be seen from figure 4.3, the peak indicates where a high accumulation is exhibited. The size of the positron source is estimated by comparing the size of the smallest circle of the contour with the size with the size of the square on the grid (5×5) cm^2. I found that the size is about 5 cm in diameter. The position was also found to be at the center of the body as it is indicated by the green circle on the plot.

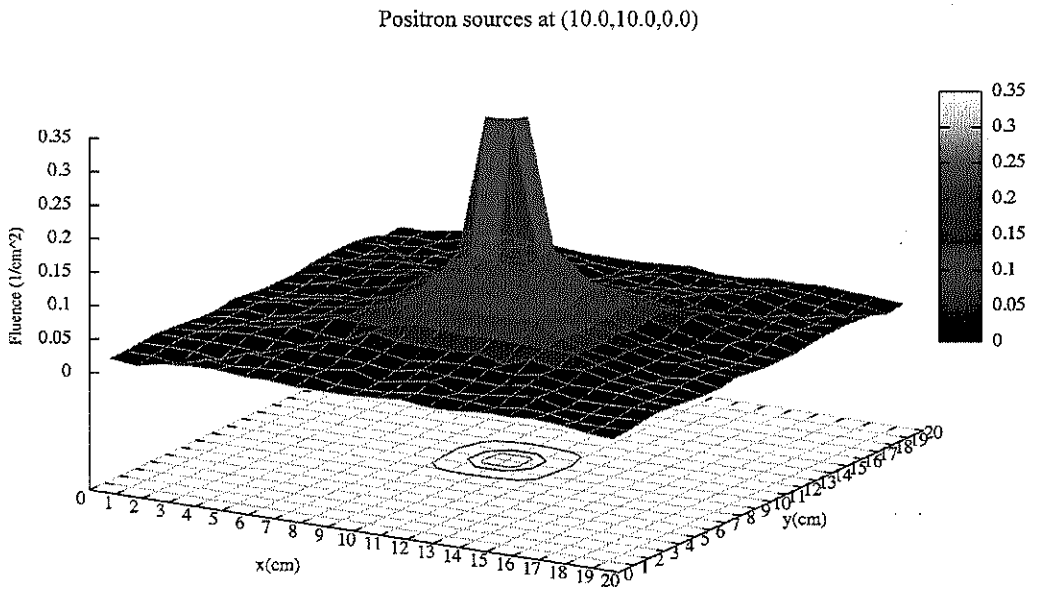

Figure 4.3. Positron sources located at (10.0,10.0,0.0). Silicon is used as detector material. The size of the source is estimated by the size of the ring corresponds to the highest peak of the flux distribution. * 1 division=5 cm

Secondly, I moved the positron source slightly away from the center (at 11.0,11.0,0.0) of the body phantom and repeated the calculation for the position as well as estimating the size. In this case I found that the position and the size of the positron source as it was expected, figure 4.4.

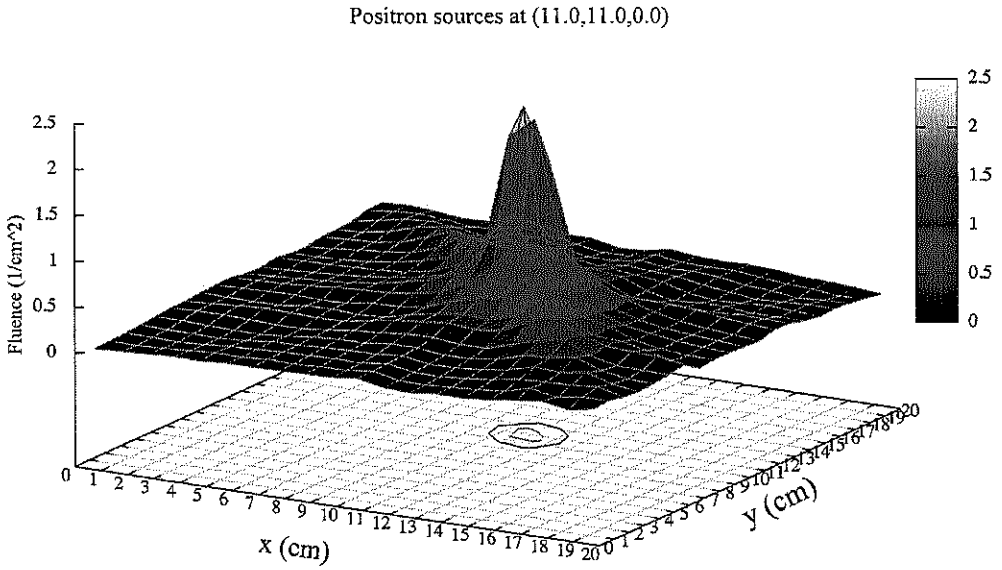

Figure 4.4. Positron sources located at (11.0,11.0,0.0). Silicon is used as detector material. The size of the source is estimated by the size of the ring corresponds to the highest peak of the flux distribution. * 1 division=5 cm

To see how accurate the method that has been used to estimate the size of the positron source and its position, the positron source was moved far away from the ceneter (at 8.0,8.6,0.0) of body phantom. The position of the source was accurate, whereas, the size of the positron source was slightly larger. This can be clearly seen from figure 4.5.

Finally, I changed the material of the detector (silicon with BGO) in order to see if there were any differeces comparing the last case (positron source at 8.0,8.6,0.0) when the silicon was used as detector material. The first thing that was noticed is that the counting rate of the coincidences increased.

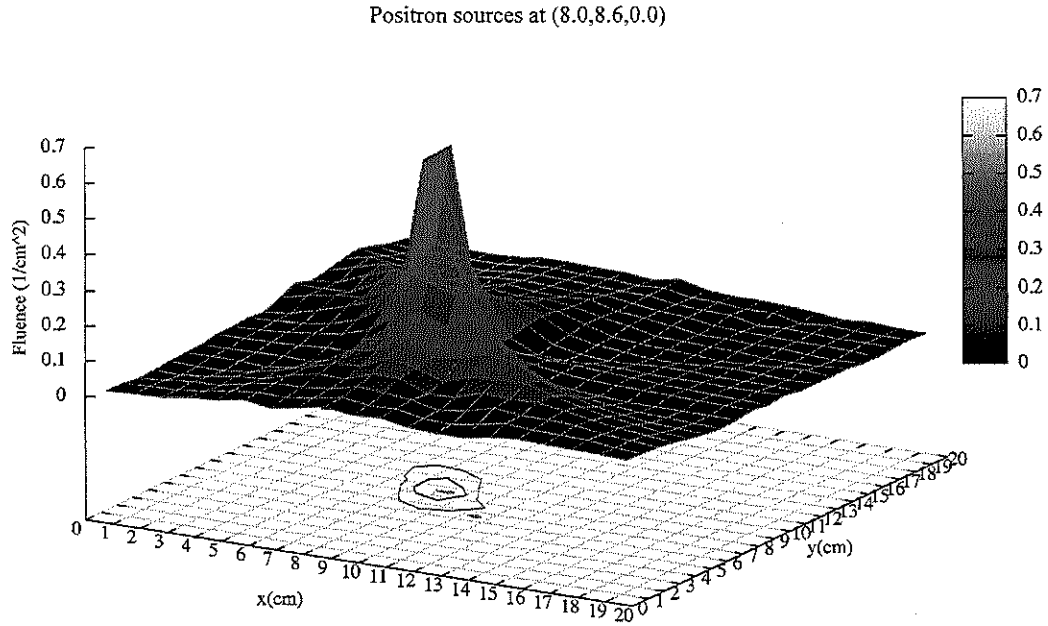

Figure 4.5. Positron sources located at (8.0,8.6,0.0). Silicon is used as detector material. The size of the source is estimated by the size of the ring corresponds to the highest peak of the flux distribution. * 1 division=5 cm

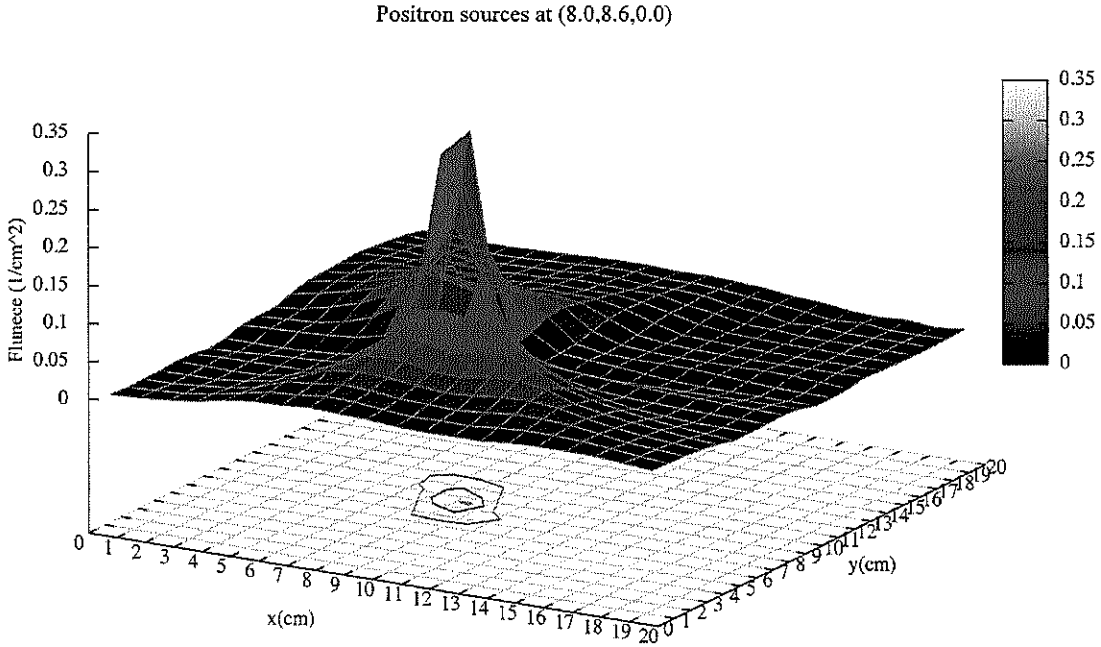

Figure 4.6. Positron sources located at (8.0,8.6,0.0). BGO is used as detector material. The size of the source is estimated by the size of the ring corresponds to the highest peak of the flux distribution. * 1 division=5 cm

Even after changing the hight of the detectors I still get a bettter counting rate compared to the other case when using silicon as detector material. This gives an advantage when considering thinner slices of the scanned object.

4.2 Dose-Equivalent Calculation

Generally, the dose that patients receive when performing a PET scan is due to the energy deposited by γ-ray photons. The uptaken dose (coming from the radiopharmaceutical) is very important. The effecticve dose the patients would get from ^{18}FDG is about 1mSv [4, p. 373]. I calculated the dose equivalent in the region surrounding the positron source. The region where the positron source resides is not of interest since the positrons do not traversing long distances (few millimeters) within the regions surrounding the cancerous tumor. It is important to know how much dose a patient can get from γ-ray radiation emitted after the annihilation of the positrons. At time zero, the total number of the positrons is N_0. After time "t" this number is given by:

$$N = N_0 e^{\frac{-t}{\tau}} \tag{4.1}$$

Where t is the time of decay, and τ is the mean life time. In this project I calculated the dose equivalent for fluorine dioxide glucose (FDG). It has half-life time ($T_{1/2}$) of 110 minutes, where, $\tau = \frac{T_{1/2}}{ln2}$ =158.69 minutes.

$$\frac{dN}{dt} = -\frac{1}{\tau} N_0 e^{\frac{-t}{\tau}}$$

$$\Delta N = -\frac{1}{\tau} N_0 \int_{t_1}^{t_2} e^{\frac{-t}{\tau}} dt \tag{4.2}$$

$$\Delta N = -N_0 (e^{\frac{-t_2}{\tau}} - e^{\frac{-t_1}{\tau}})$$

$$\Rightarrow \frac{\Delta N}{N_0} = (e^{\frac{-t_1}{\tau}} - e^{\frac{-t_2}{\tau}}) \tag{4.3}$$

And this is the contribution ratio of the positrons to the dose equivalent during the time of the scan. Typically, patients stay for 60 minutes after adminstrating the radionuclide before performing the scan. PET scans usaully take about 20-30 mintues for a full scan. Subtituting in equation (4.3) by 60 and 80 minutes for t_1 and t_2 respectively, gives $\frac{\Delta N}{N_0} = 0.0811$. This ratio represents 8.11% of the total amount of positrons contribution to the dose equivalent during the time of scan, and therefore, for the total dose equivalent mutlipy by $(\frac{1}{0.0811})$ or 12.33 to account for the total equivalent dose. It has been calculated in Appendix B, and it was found to be equal to 80.33 μSv. This amount of dose is relatively small as compared to the Internation Comission of Radiation Protection (ICRP). According to the ICRP publication [21], the annual effective dose for general public averaged over 5 years is 1.0 mSv.

CHAPTER V

CONCLUSION AND OUTLOOK

PET is becoming one of the most important and common nuclear medicine imaging methods that in oncology, monitoring brain activities, assessing the advancement the cancer. In this project, I demonstrated the positron source of (cancerous tumor) located at different positions inside a body phantom. The location and size of the positron source was estimated by calculating the line segments that cross each cell on the grid shown in figure 4.1 as a measure of the γ-ray fluence contributions. Using a γ-ray fluence calculation for source shape and position reconstruction gives a reasonable resolution. In both detector materials (Silicon and BGO) that have been used, the position of the positron source was located precisely.

The size of the source was not as expected as the source was shifted far from the center from the square detector array. This might be related to the field of view (FOV), thus, as you move the positron source closer to one of the square array detector sides, the FOV gets smaller at that side as compared to the others.

For the BGO detector, the number of positron particles generated was less than that in the case of silicon. This is because the BGO has higher efficiency than the silicon. In addition, the stopping power for BGO is higher. Also BGO has a shorter dead-time (900–1200 ns), and this increases the efficiency of counting the coincidence events. Therfore, BGO is used in most PET systems.

In dose equivalent calculation, the results of the simulation were reasonable as compared to the ICRP regulation. Therefore, for the given dose in this project, a secondary cancer risk is not likely be resulted.

Future studies should include a finer grid for better resolution. What meant by finer grids is that the dimensions of the detector array elements are small (few millimeters) in order to have a

large number of pixels on the grid. Also a circular array of detectors should be investigated using the principle of γ-ray fluence to estimate the size and the position of the positron source.

APPENDICES

APPENDIX A

FLUKA INPUT

This appendix contains the input file of FLUKA Code simulation setup. The command lines in FLUKA input file set up are introduced through cards, and each card is described by key words given in what called "WAHTs", six floating point values. The seventh WHAT called SDUM and it is to give names to some cads (e.g., USRBIN cards) or to declare some features such as PRECISION, etc. Not all WAHTs are used as it will be been below.

```
*...+....1....+....2....+....3....+....4....+....5....+....6....+....7....+....8
TITLE
                          Spherical Positron Source
* ..+....1....+....2....+....3....+....4....+....5....+....6....+....7....+....8
GLOBAL     2000.        -1.          1.          0.
```

The GLOBAL card is used to declare some important parameters such as, the maximum number of regions, and if run is analog or biased. In this input file the run is chosen to be analogue (WAHT (2) $<$ 1.0 for analog and WAHT (2) $>$ 1.0 for biasing). WHAT(3) declares DNEAR (the distance between the current particle position and the nearest boundary). WHAT(4) flags request various types of input (WHAT(4) = 0.0 means ignored).

```
* ..+....1....+....2....+....3....+....4....+....5....+....6....+....7....+....8
DEFAULTS                                                              PRECISIO
```

DEFAULTS card sets FLUKA defaults that are suitable for a particular type of problems. In this input file FLUKA defaults have been sat up for precision. It activates the electromagnetic field, Rayleigh scattering and inelastic form factor corrections to Compton scattering, photoelectric edge treatment, and some other defaults.

```
BEAM       -634.E-06        0.0 6283.1185        0.0        0.0       1.0POSITRON
BEAMPOS          5.0        5.0        0.0        0.0        0.0
BEAMPOS          0.0        2.5        0.0        0.0        0.0       0.0SPHE-VOL
```

BEAM and BEAMPOS cards are used to set up the properties of the particle source (beam). BEAM card sets the beam energy, divergence type (Gaussian angular distribution or isotropic distribution), direction, and shape of the beam. BEAMPOS sets the beam coordinates (from which particles transport starts) direction. Two BEAMPOS cards can be used to specify a spatially extended source shaped by setting the SDUM to the desired shape (in this input file I used shperical shape source; SDUM=PHE-VOL). In this project, I defined a positrons surce of -634.E-06 GeV (WHAT(1)); the minus sign defines the averagy kinetic energy. Beam divergence is isotropic in 360^0. (WHAT(3)=6283.1185).

```
GEOBEGIN                                                              COMBNAME
    0    0                  Geometry setup of the target
RPP bhole      -5000.0 +5000.0 -5000.0 +5000.0 -5000.0 +5000.0
RPP vacum      -1000.0 +1000.0 -1000.0 +1000.0 -1000.0 +1000.0
RPP air        -500.0 +500.0 -500.0 +500.0 -500.0 +500.0
RPP body       -10.0 +10.0 -10.0 +10.0 -10.0 10.0
RPP xr1        50.0 54.0 -50.0 -45.0 -10.0 10.0
.
.
RPP ydo20    45.0 50.0 -54.0 -50.0 -10.0 10.0
*
END
```

The combinatorial geometry such as, bodies, regions are introduced through the GEOBEGIN and GEOEND cards. The body type is introduced via commmad lines (e.g., RPP, REC, RCC, BOX, SPH, etc.) The surrounding environment of the geometry simulation is particle lost cavity (black-hole), vacuum cavity, and air cavity from outside-in respectively. In this project I used recangular parallelpipe (RPP) bodies. The names immediately follow after the body type command (e.g., bhole, vacum, etc.) The dimensions are described by WHAT(2-6) as follow: x_min, x_max, y_min, y_max, z_min, z_max respectively. For simplicity the coordinates were chosen to be symmetric around the origin.

```
* black hole
Blkhole   5     +bhole  -vacum
* vacuum around
```

```
Vacc      5     +vacum  -air
* air cavity
Aire      5     +air    -body  -xr1  -xr2  -xr3 -xr4 -xr5 ....
                     ................................ -ydo20
.
.
Dt80     85     +ydo20
END
GEOEND
```

It is very important to specify the regions of the bodies and the surrounding environment and give them names, e.g., Blkhole, Vacc, etc., in order to assign their material. The upper limit of the region is designated by (+), where, the lower limt that is going to be substcated is designated by (-) (e.g, +vacum -air).

```
*...+....1....+....2....+....3....+....4....+....5....+....6....+....7....+....8
MATERIAL         0.0       0.0       1.0        26       0.0       0.0  WATER
MATERIAL         14.    28.0855     2.329        27       0.0       0.0  SILICON
COMPOUND     2.0    HYDROGEN       1.0    OXYGEN       0.0       0.0  WATER
MATERIAL         0.0       0.0  0.001205       28.       0.0       0.0  AIR
COMPOUND   -0.000124    CARBON -0.755267  NITROGEN -0.231781    OXYGEN  AIR
COMPOUND   -0.012827     ARGON                                         AIR
```

MATERIAL and COMPOUND cards are used to describe the materials that will be assigned for the bodies and regions. A compound material can be created by combining the two cards, MATERIAL and COMPOUND; where the SDUM has the same name of the desired compound, e.g., AIR, WATER.

```
ASSIGNMAT        AIR      Aire
*  External Black Hole
ASSIGNMAT   BLCKHOLE   Blkhole
*  Vacuum
ASSIGNMAT    VACUUM     Vacc
* Assigning materials to Body
ASSIGNMAT      WATER      Bodd
* Detector Materials
ASSIGNMAT    SILICON       Dt1
.
.
.
.
ASSIGNMAT    SILICON      Dt80
```

ASSIGNMAT cards assign the materials, compounds to the bodies or regions. It simply has two importanat key words, WHAT(1) is the name of the material or compound that has been created using MATERIAL, COMPOUND cards, and the region name WHAT (2) is specified within the geometry cards. In this project, I assigned water for body phantom, and silicon for detector material.

```
* ************************    DETECTOR CARDS   ******************************
*...+....1....+....2....+....3....+....4....+....5....+....6....+....7....+....8

DETECT          0.0     1.E-9     1.E-3     5.E-4       1.0      Dt01  01
DETECT          0.0     -Dt21                                          &

.
.
.
DETECT          0.0     1.E-9     1.E-3     5.E-4       1.0      Dt01  10
DETECT          0.0     -Dt30                                          &
```

DETECT card provides coincidence and anti-coincidence capability by using energy deposition scoring on event by event basis. WHAT(1) = 0.0 for a detector.

WHAT(2) = Lower limit of total energy being scored in the detector regions in one event.

WHAT(3) = upper limit of total energy being scored in the detector regions in one event.

WHAT(4) = cutoff energy for the signal (coincidence or anticoincidence threshold).

WHAT(5) = > 0.0 : the detector regions are considered to be in COINCIDENCE with the trigger regions.

WHAT(6) = region number or name preceded by a (-) is considered to be first region of the DETECTOR. Region number or name preceded by a (-) is considered to be the first region of the TRIGGER.

For the continuation card the SDUM = &

WHAT(1) = same as WHAT(1) for the first card.

WHAT(2-6) = following regions (with sign). If not preceded by a minus sign, they are considered detector regions, otherwise trigger regions.

```
RANDOMIZE         1.0
*...+....1....+....2....+....3....+....4....+....5....+....6....+....7....+....8
START           100E6
STOP
```

RANDOMIZE card sets the logical unit for the random number generator.

START card defiens the number of histories (particles need to ne generated).

APPENDIX B

Dose Calculation

This appendix is the output of dose equivalent simulation given in equivalent dose calculation section.

```
***** Spherical Positron Source For Dose Calculation *****
DATE: 5/ 9/12, TIME: 12: 1:27
Total number of particles followed 100000000, for a total weight of 1.0000E+08
```

The volume of interst for the USRBINS binning can be described in Cartesian or cylindrical coordinates. I used Cartesian coordinates and the dimesnsions were chosen to be 1 cm in all directions (1 cm^3). The scoring results are writen from the lower limit to the uper limit of the user defined dimension of the USRBIN.

```
Cartesian binning n. 1 " d_eq1 " , generalized particle n. 240
X coordinate: from -5.0000E-01 to 5.0000E-01 cm, 1 bins ( 1.0000E+00 cm wide)
Y coordinate: from -5.0000E-01 to 5.0000E-01 cm, 1 bins ( 1.0000E+00 cm wide)
Z coordinate: from 4.2500E+01 to 4.3500E+01 cm, 1 bins ( 1.0000E+00 cm wide)
Data follow in a matrix A(ix,iy,iz), format (1(5x,1p,10(1x,e11.4)))
accurate deposition along the tracks requested
this is a track-length binning
6.5153E-02
```

Where, *6.5153E-02*, is the dose equivalent expressed in pSv per unit total number of particles (primary weight). Therefore, I need to multipy by the total weight (total number of particles generated) to account for dose equivalent in terms of Sv.

Dose-EQ= (1.0E+08* 6.5153E-02*1.0E-12) Sv=6.5153E-6 Sv And this represents the dose during the time of scan (20 minutes). As disscussed in section 4.2, this value needs to be multiplied by 12.33 in order to get the total dose equivalent. Thus: Dose-EQ_{tot}= 12.33*6.5153E-6 Sv =80.33 μSv

REFERENCES

[1] M. Wernich and J. Aarsvold, *Emission Tomography: Fundamentals of PET and SPECT*. Elsevier Inc, London, Uk (2004).

[2] C. Leondes (ed.), *Medical Imaging Systems Techniques and Applications: General Anatomy*. Gordon And Breach Science, Amsterdam, The Netherlands (1997).

[3] R. Badawi, *Aspects of optimisation and quantification in three dimensional positron emission tomography*. Ph.D. thesis, University of London (1998).

[4] F. Mettler and M. Guiberteau, *Essentials of Nuclear Medicine Imaging*. 5th ed., Saunders Elseviers, Philadelphia, PA (2006).

[5] D. Delbeke, W. Martin, J. Patton and M. Sandler, *Practical FDG Imaging : A Teaching File*. Springer, New York, NY (2002).

[6] S. Kane, *Introduction To Physics In Modern Medicine*. 2nd ed., Taylor & Francis Group, New York, NY (2009).

[7] G. Muehllehner and J. Karp, *Positron emission tomography*. Physics In Medicine And Biology 51, R117–R137 (2006).

[8] E. Lin and A. Abass (eds.), *PET And PET/CT: A Clinical Guide*. Thieme, New York, NY (2005).

[9] G. Saha, *Basics of PET Imaging: Physics, Chemistry, and Regulations*. Springer, New York, NY (2005).

[10] D. Bailey, D. Townsend, P. Valk and M. Maiseya (eds.), *Positron Emission Tomography: Basic Sciences*. Springer, London, UK (2005).

[11] Z. Cho, J. Jones and M. Singh, *Foundations of Medical Imaging*. John Wiley & Sons, New York, NY (1993).

[12] J. Martin, *Physics for Radiation Protection: A Handbook*. 2nd ed., John Wiley & Sons, Oxford, UK (2006).

[13] G. Saha, *Physics and Radiobiology of Nuclear Medicine*. 3rd ed., Springer, New York, NY (2006).

[14] S. Cherry, J. Sorenson and M. Phelps, *Physics in Nuclear Medicine*. Saunders Elsevier Science, Philadelphia, PA (2003).

[15] G. Knoll, *Radiation Detection And Measurement*. 3th ed., John wiley & Sons Inc, New York, NY (2000).

[16] E. Alpen, *Radiation Biophysics*. Prentice Hall Inc, New Jersey, NJ (1990).

[17] E. Hall and A. Giaccia, *Radiobiology For The Radiologist*. 6th ed., Lippincott Williams & Wilkins, Philadelphia, PA (2006).

[18] A. Klein and A. Godunov, *Introductory Computational Physics*. Cambridge University Press, New York, NY (2006).

[19] A. Ferrari, A. Fasso, J. Ranft and P. Sala, *Fluka: a multi-particle transport code* (2000-2012), URL `http://www.fluka.org`.

[20] H. Bingsheng, L. Martin W. and K. Pek-Lan, *Whole-body pet/ct scanning: Estimation of radiation dose and cancer risk.* Medical Physics 251, 166–174 (2009).

[21] N. Petoussi-Henss, W. E. Bolch, K. F. Eckerman, A. Endo, N. Hertel, J. Hunt, M. Pelliccioni, H. Schlattl, M. Zankl, International Commission on Radiological Protection and International Commission on Radiation Units and Measurements, *Conversion coefficients for radiological protection quantities for external radiation exposures.* Ann ICRP 40, 1–257 (2010).